Spatiotemporal chaos in terms of unstable recurrent patterns

Nonlinearity **10** (1997) 55–70. Printed in the UK PII: S0951-7715(97)75987-5

Spatiotemporal chaos in terms of unstable recurrent patterns

F Christiansen†, P Cvitanović and V Putkaradze

Centre for Chaos and Turbulence Studies, Niels Bohr Institute, Blegdamsvej 17, DK-2100 Copenhagen Ø, Denmark

Received 3 July 1996
Recommended by H Levine

Abstract. Spatiotemporally chaotic dynamics of a Kuramoto–Sivashinsky system is described by means of an infinite hierarchy of its unstable spatiotemporally periodic solutions. An intrinsic parametrization of the corresponding invariant set serves as an accurate guide to the high-dimensional dynamics, and the periodic orbit theory yields several global averages characterizing the chaotic dynamics.

PACS numbers: 0230J, 0320, 0340, 0545

Introduction

In recent years unstable periodic orbits have been shown to be an effective tool in the description of deterministic dynamical systems of low intrinsic dimension [1], in diagnosing deterministic chaos in noisy biological systems [2], and many other applications. The theory has been successfully applied to low-dimensional ordinary differential equations (deterministic chaos) and linear partial differential equations (semiclassical quantization). It is an open question whether the theory has anything to say about nonlinear partial differential equations (hydrodynamics, field theory). In this paper we show that the periodic orbit theory can be used to describe spatially extended systems by applying it to the Kuramoto–Sivashinsky equation [3, 4].

In what follows we shall refer to a periodic solution as a 'cycle', and to the closure of the union of all periodic solutions as the 'invariant set'. Periodic solutions are important because they form the skeleton of the invariant set [5, 6], with cycles ordered hierarchically; short cycles give good approximations to the invariant set, longer cycles refinements. Errors due to neglecting long cycles can be bounded, and for nice hyperbolic systems they fall off exponentially or even superexponentially with the cut-off cycle length [7, 8]. Furthermore, cycles are structurally robust as for smooth flows eigenvalues of short cycles vary slowly with smooth parameter changes, short cycles can be accurately extracted from experimental or numerical data, and global averages (such as correlation exponents, escape rates and other 'thermodynamic' averages) can be efficiently computed from short cycles by means of cycle expansions.

† Current address: Max-Planck-Institut für Physik komplexer Systeme, Bayreuther Strasse 40, Haus 16, D-01187 Dresden, Germany.

0951-7715/97/000055+16$19.50

While the role of periodic solutions in elucidating the asymptotics of ordinary differential equations was already appreciated by Poincaré [9], allegedly Hopf [10] and, more demonstrably, Spiegel and collaborators [11–13] have argued that the asymptotics of partial differential equations should also be described in terms of recurrent spatiotemporal patterns. Pictorially, dynamics drives a given spatially extended system through a repertoire of unstable patterns; as we watch a given 'turbulent' system evolve, every so often we catch a glimpse of a familiar pattern. For any finite spatial resolution, the system follows approximately for a finite time a pattern belonging to a finite alphabet of admissible patterns, and the long term dynamics can be thought of as a walk through the space of such patterns, just as chaotic dynamics with a low-dimensional attractor can be thought of as a succession of nearly periodic (but unstable) motions.

1. Kuramoto–Sivashinsky system

We offer here a modest implementation of the above program on a prototype spatially extended dynamical system defined by the Kuramoto–Sivashinsky equation [3, 4]

$$u_t = (u^2)_x - u_{xx} - \nu u_{xxxx} \tag{1}$$

which arises as a model amplitude equation for interfacial instabilities in a variety of contexts—see e.g. [14]. Here $t \geqslant 0$ is the time, $x \in [0, 2\pi]$ is the space coordinate, and ν is a fourth-order 'viscosity' damping parameter. The subscripts x and t denote the partial derivatives with respect to x and t. We take the Kuramoto–Sivashinsky system because it is one of the simplest physically interesting spatially extended nonlinear systems, but in the present context the interpretation of the equation, or the equation itself is not the most important element; the approach should be applicable to a wide class of spatially extended nonlinear systems. The salient feature of such partial differential equations is that for any finite value of ν their asymptotics is in principle describable by a *finite* set of 'inertial manifold' ordinary differential equations [15].

The program of studying unstable solutions in this context was initiated by Goren, Eckmann and Procaccia [16] who have used a two-unstable modes truncation of the Kuramoto–Sivashinsky equation to study the dynamics connecting coexisting unstable *temporally stationary* solutions. We shall study here unstable *spatiotemporally periodic* solutions of the *full* Kuramoto–Sivashinsky system. Our main result is that in the limit of weak turbulence or 'spatiotemporal chaos', we can determine hierarchically and exhaustively cycles of longer and longer periods, and apply this data to the evaluation of global averages.

The function $u(x, t) = u(x + 2\pi, t)$ is assumed periodic on the $x \in [0, 2\pi]$ interval. As $u(x, t)$ has compact support, the standard strategy is to expand it in a discrete spatial Fourier series:

$$u(x, t) = \sum_{k=-\infty}^{+\infty} b_k(t) \mathrm{e}^{\mathrm{i}kx}. \tag{2}$$

Since $u(x, t)$ is real, $b_k = b_{-k}^*$. Substituting (2) into (1) yields the infinite ladder of evolution equations for the Fourier coefficients b_k:

$$\dot{b}_k = (k^2 - \nu k^4) b_k + \mathrm{i}k \sum_{m=-\infty}^{\infty} b_m b_{k-m}. \tag{3}$$

As $\dot{b}_0 = 0$, the average (the mean drift) of the solution is an integral of motion. In what follows we shall assume that this average is zero, $\int \mathrm{d}x\, u(x, t) = 0$.

The coefficients b_k are in general complex functions of time. We can simplify the system (3) further by assuming that b_k are pure imaginary, $b_k = \mathrm{i}a_k$, where a_k are real. As we shall see below, this picks out the subspace of odd solutions $u(x,t) = -u(-x,t)$, with the evolution equations

$$\dot{a}_k = (k^2 - \nu k^4)a_k - k \sum_{m=-\infty}^{\infty} a_m a_{k-m}. \tag{4}$$

We shall determine the periodic solutions in the space of Fourier coefficients, and then reconstitute from them the unstable spatiotemporally periodic solutions of (1).

The trivial solution $u(x,t) = 0$ is a fixed point of (1). From (4) it follows that the $|k| < 1/\sqrt{\nu}$ long wavelength modes of this fixed point are linearly unstable, and the $|k| > 1/\sqrt{\nu}$ short wavelength modes are stable. For $\nu > 1$, $u(x,t) = 0$ is the globally attractive stable fixed point; starting with $\nu = 1$ the solutions go through a rich sequence of bifurcations, studied e.g. in [14]. Detailed knowledge of the parameter dependence of bifurcations sequences is not needed for our purposes; we shall take $\sqrt{\nu}$ sufficiently small so that the dynamics can be spatiotemporally chaotic, but not so small that we would be overwhelmed by too many short wavelength modes needed in order to accurately represent the dynamics.

The growth of the unstable long wavelengths (low $|k|$) excites the short wavelengths through the nonlinear term in (4). The excitations thus transferred are dissipated by the strongly damped short wavelengths, and a sort of 'chaotic equilibrium' can emerge. The very short wavelengths $|k| \gg 1/\sqrt{\nu}$ will remain small for all times, but the intermediate wavelengths of order $|k| \sim 1/\sqrt{\nu}$ will play an important role in maintaining the dynamical equilibrium. As the damping parameter decreases, the solutions increasingly take on Burgers type shock front character which is poorly represented by the Fourier basis, and many higher harmonics need to be kept [14, 16] in truncations of (4). Hence, while one may truncate the high modes in the expansion (4), care has to be exercised to ensure that no modes essential to the dynamics are chopped away.

Before proceeding with the calculations, we take into account the symmetries of the solutions and describe our criterion for reliable truncations of the infinite ladder of ordinary differential equations (4).

2. Symmetry decomposition

As usual, the first step in analysis of such dynamical flows is to restrict the dynamics to a Poincaré section. We shall fix the Poincaré section to be the hyperplane $a_1 = 0$. We integrate (4) with the initial conditions $a_1 = 0$, and arbitrary values of the coordinates $a_2, \ldots, a_N$, where N is the truncation order. When a_1 becomes 0 the next time, the coordinates $a_2, \ldots, a_N$ are mapped into $(a_2', \ldots a_N') = P(a_2, \ldots, a_N)$, where P is the Poincaré map. P defines a mapping of a $(N-1)$-dimensional hyperplane into itself. Under successive iterations of P, any trajectory approaches the attractor $\mathcal{A}$, which itself is an invariant set under P.

A trajectory of (4) can cross the plane $a_1 = 0$ in two possible ways: either when $\dot{a}_1 > 0$ ('up' intersection) or when $\dot{a}_1 < 0$ ('down' intersection), with the 'down' and 'up' crossings alternating. It then makes sense to define the Poincaré map P as a transition between, say, 'up' and 'up' crossing. With Poincaré section defined as the 'up–up' transition, it is natural to define a 'down–up' transition map Θ. Since Θ describes the transition from down to up (or up to down) state, the map Θ^2 describes the transition up–down–up, that is $\Theta^2 = P$.

Consider the spatial flip and shift symmetry operations $Ru(x) = u(-x)$, $Su(x) = u(x+\pi)$. The latter symmetry reflects the invariance under the shift $u(x,t) \to u(x+\pi,t)$, and is a particular case of the translational invariance of the Kuramoto–Sivashinsky equation (1). In the Fourier modes decomposition (4) this symmetry acts as $S : a_{2k} \to a_{2k}, a_{2k+1} \to -a_{2k+1}$. Relations $R^2 = S^2 = 1$ induce decomposition of the space of solutions into four invariant subspaces [14]; the above restriction to $b_k = \mathrm{i}a_k$ amounts to specializing to a subspace of odd solutions $u(x,t) = -u(-x,t)$.

Now, with the help of the symmetry S the whole attractor $\mathcal{A}_{tot}$ can be decomposed into two pieces: $\mathcal{A}_{tot} = \mathcal{A}_0 \cup S\mathcal{A}_0$ for some set $\mathcal{A}_0$. It can happen that the set $\mathcal{A}_0$ (the symmetrically decomposed attractor) can be decomposed even further by the action of the map Θ. In this case the attractor will consist of four disjoint sets: $\mathcal{A}_{tot} = \mathcal{A} \cup S\mathcal{A} \cup \Theta\mathcal{A} \cup \Theta S\mathcal{A}$. As we shall see, this decomposition is not always possible, since sometimes $\mathcal{A}$ overlaps with $\Theta S\mathcal{A}$ (in this case $\Theta\mathcal{A}$ will also overlap with $S\mathcal{A}$). We shall carry out our calculations in the regime where the decomposition into four disjoint pieces is possible. In this case the set $\mathcal{A}$ can be taken as the fundamental domain of the Poincaré map, with $S\mathcal{A}$, $\Theta\mathcal{A}$ and $\Theta S\mathcal{A}$ its images under the S and Θ mappings.

This reduction of the dynamics to the fundamental domain is particularly useful in periodic orbit calculations, as it simplifies symbolic dynamics and improves the convergence of cycle expansions [17].

3. Fourier modes truncations

When we simulate the equation (4) on a computer, we have to truncate the ladder of equations to a finite length N, i.e. set $a_k = 0$ for $k > N$. N has to be sufficiently large that no harmonics a_k important for the dynamics with $k > N$ are truncated. On the other hand, computation time increases dramatically with the increase of N: since we will be evaluating the stability matrices for the flow, the computation time will grow at least by N^2.

Adding an extra dimension to a truncation of the system (4) introduces a small perturbation, and this can (and often will) throw the system into a totally different asymptotic state. A chaotic attractor for $N = 15$ can become a period-3 window for $N = 16$, and so on. If we compute, for example, the Lyapunov exponent $\lambda(\nu, N)$ for the strange attractor of the system (4), there is no reason to expect $\lambda(\nu, N)$ to smoothly converge to the limit value $\lambda(\nu, \infty)$ as $N \to \infty$. The situation is different in the periodic windows, where the system is structurally stable, and it makes sense to compute Lyapunov exponents, escape rates, etc for the *repeller*, i.e. the closure of the set of all *unstable* periodic orbits. Here the power of cycle expansions comes in: to compute quantities on the repeller by direct averaging methods is generally more difficult, because the motion quickly collapses to the stable cycle.

We have found that the minimum value of N to get any chaotic behaviour at all was $N = 9$. However, the dynamics for the $N = 9$ truncated system is rather different from the full system dynamics, and therefore we have performed our numerical calculations for $N = 15$, $N = 16$ and $N = 17$. Figure 1 is a representative plot of the Feigenbaum tree for the Poincaré map P. To obtain this figure, we took a random initial point, iterated it for a some time to let it settle on the attractor and then plotted the a_6 coordinate of the next 1000 intersections with the Poincaré section. Repeating this for different values of the damping parameter ν, one can obtain a picture of the attractor as a function of ν. For an intermediate range of values of ν, the dynamics exhibits a rich variety of behaviours, such as strange attractors, stable limit cycles, and so on. The Feigenbaum trees for different values of N resemble each other, but the precise values of ν corresponding the various

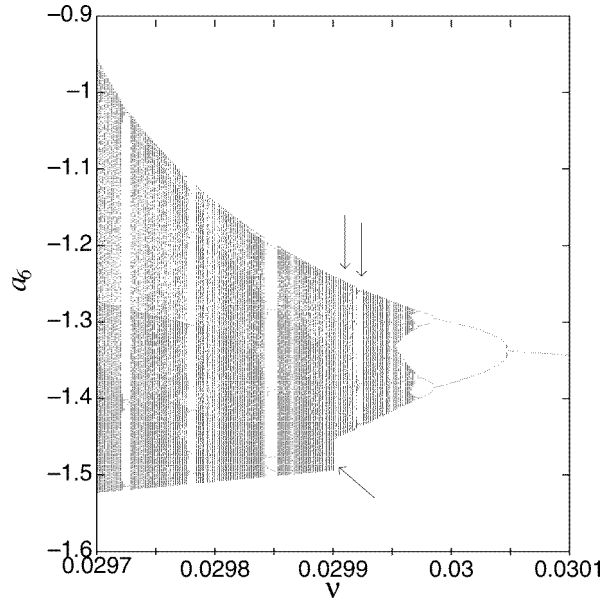

Figure 1. Feigenbaum tree for coordinate a_6, $N = 16$ Fourier modes truncation of (4). The two upper arrows indicate the values of damping parameter that we use in our numerical investigations; $\nu = 0.029\,910$ (chaotic) and $\nu = 0.029\,924$ (period-3 window). The lower arrow indicates the kink where the invariant set $\mathcal{A}$ starts to overlap with $\Theta S\mathcal{A}$. Truncation to $N = 17$ modes yields a similar figure, with values for specific bifurcation points shifted by $\sim 10^{-5}$ with respect to the $N = 16$ values. The choice of the coordinate a_6 is arbitrary; projected down to any coordinate, the tree is qualitatively the same.

bifurcations depend on the order of truncation N.

Based on the observed numerical similarity between the Feigenbaum trees for $N = 16$ and $N = 17$ (cf. figure 1), we choose $N = 16$ as a reasonable cut-off and will use only this truncation throughout the remainder of this paper. We will examine two values of the damping parameter: $\nu = 0.029\,910$, for which the system is chaotic, and $\nu = 0.029\,924$, for which the system has a stable period-3 cycle. In our numerical work we use both the pseudospectral [18] and the fourth order variable-step Runge–Kutta integration routines [19]; their results are in satisfactory agreement. As will be seen below, the good control of symbolic dynamics guarantees that we do not miss any short periodic orbits generated by the bifurcation sequence indicated by the Feigenbaum tree of figure 1. However, even though we are fairly sure that for this parameter value we have all short periodic orbits, the possibility that other sets of periodic solutions exist somewhere else in the phase space has not been excluded.

The problem with such high-dimensional truncations of (4) is that the dynamics is difficult to visualize. We can examine its projections onto any three axes a_i, a_j, a_k, as in figure 2 or, alternatively, study a return map for a given coordinate $a_k \to a'_k = P_k(a_2, \ldots, a_N)$ as the one plotted in figure 3. The full return map is $(N-1)$-dimensional $\boldsymbol{a} \to \boldsymbol{P}(a_2, \ldots, a_N) = \boldsymbol{a}'$ and single-valued, and for the values of ν used here the attractor is essentially one-dimensional, but its projection into the $\{a_k, P_k(a_2, \ldots, a_N)\}$ plane can be multi-valued and self-intersecting. One can imagine a situation where no 'good' projection is possible, that is, any projection onto any two-dimensional plane is a multiple-valued function. The question is how to treat such a map?

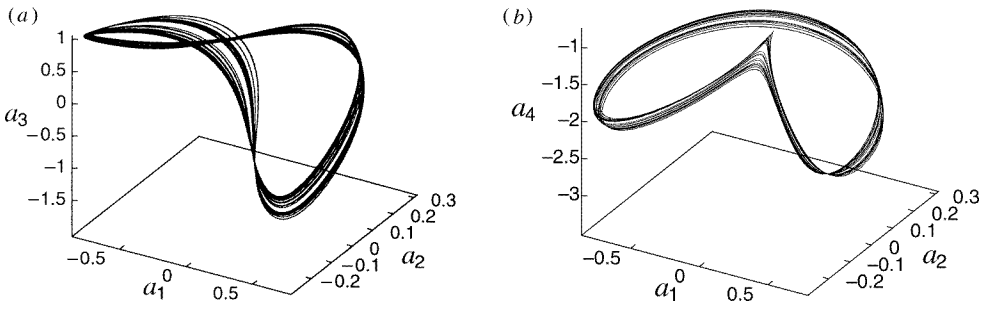

Figure 2. Projections of a typical 16-dimensional trajectory onto different three-dimensional subspaces, coordinates (*a*) $\{a_1, a_2, a_3\}$, (*b*) $\{a_1, a_2, a_4\}$. $N = 16$ Fourier modes truncation with $\nu = 0.029\,910$.

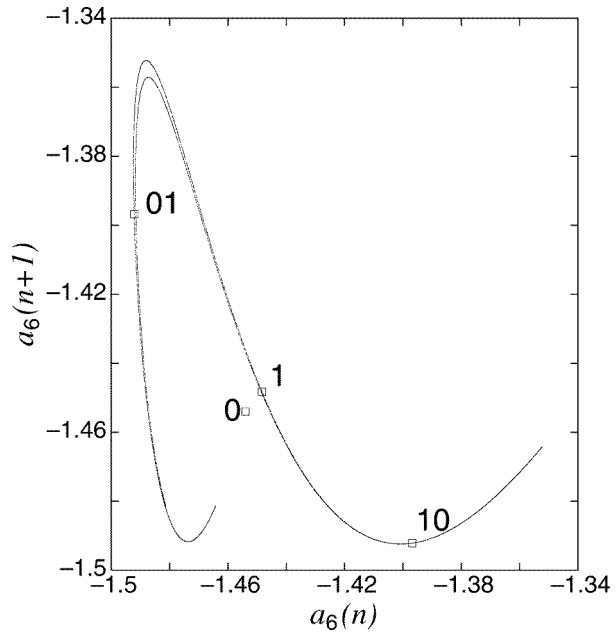

Figure 3. The attractor of the system (4), plotted as the a_6 component of the $a_1 = 0$ Poincaré section return map, 10 000 Poincaré section returns of a typical trajectory. Indicated are the periodic points $\overline{0}$, $\overline{1}$ and $\overline{01}$; as this is an arbitrary projection of the invariant set, they exhibit no good spatial ordering. $N = 16$ Fourier modes truncation with $\nu = 0.029\,910$.

4. One-dimensional visualization of the dynamics

We now describe an approach which simplifies matters a lot by reducing the map to an approximate one-dimensional map. The multiple-valuedness in figure 3 arises from the fact that the return map is a two-dimensional projection of a convoluted one-dimensional curve embedded into a high-dimensional space. We shall show that it is possible to find an *intrinsic* parametrization s along the unstable manifold, such that the map $s \to f(s)$ induced by the full d-dimensional flow is approximately *one-dimensional*. Strictly speaking, the attractor on figure 3 has a certain thickness transverse to it, but the contraction in the transverse directions is so strong that the invariant set is effectively one-dimensional.

Suppose we already have determined some of the shorter cycles for our system, i.e. the fixed points of the Poincaré map and its iterates. This is accomplished relatively easily by checking a trajectory of a random initial point for close returns and then using these as initial guesses for a cycle search algorithm. We now assume that the invariant set can be approximated by a curve passing close to all periodic points, and determine the order of periodic points along such curve. This is done in the following way: there exists a fixed point which is not connected to the attractor (the point $\overline{0}$ in figure 3)—we choose this fixed point as the starting point and assign it number 1. Point number 2 is the periodic point in the sample which is closest (in the full space) to this fixed point, and the nth point is determined as the point which has the minimum distance from the point number $n-1$ among all the periodic points which have not yet been enumerated. Proceeding this way, we order all the periodic points that we have found so far.

Since all periodic points belong to cycles, their images are known and are simply the successive periodic points along the cycle. We use this fact to recursively construct a one-dimensional mapping $s_i \to f(s_i)$ (see figure 4). We approximate parametrization length s along the invariant set by computing the Euclidean inter-distances between the successive periodic points in the full dynamical space, $s_1 = 0$, $s_2 = \|\boldsymbol{a}_2 - \boldsymbol{a}_1\|$, $s_i - s_{i-1} = \|\boldsymbol{a}_i - \boldsymbol{a}_{i-1}\|$. The ith cycle point s_i is mapped onto its image $s_{\sigma i} = f(s_i)$, where σi denotes the label of the next periodic point in the cycle. We can now find longer periodic orbits of the one-dimensional map f by standard methods such as inverse iteration, and guess the location of the corresponding points in the full N-dimensional space by interpolating between the nearest known periodic points. These will not be exact periodic orbits of the full system, but are very useful as good starting guesses in a search for the exact periodic orbits. Iteratively, more and more periodic orbits can be computed. While it only pays to refine the one-dimensional parametrization until the density of the periodic points become so high that the width of the attractor becomes noticeable, the one-dimensional map continues to provide good initial guesses to longer periodic orbits. More sophisticated methods are needed only if high accuracy around the folding region of $f(s)$ is required in order to distinguish between long cycles.

For the values of ν we are working with, the attractor consists of four disjoint sets, the fundamental domain $\mathcal{A}$ and its images under the maps S and Θ. In this case the approximate return map $s \to f(s)$ is unimodal. The corresponding map on the symmetric part of the attractor, $S\Theta\mathcal{A}$, is likewise unimodal, and turned 180 degrees around the origin. For the values of ν we work with the two maps ensuring they do not interact and their domains are separate. However, if the value of the damping parameter ν is decreased sufficiently, the domains of the maps join and together they form a connected invariant set described by a bimodal map [20]. This joining of the fundamental domain $\mathcal{A}$ and its symmetric image $\Theta S\mathcal{A}$ is visible in figure 1 at $\nu \simeq 0.0299$, where the range of the a_6 coordinate increases discontinuously.

We use the unimodal map $s \to f(s)$ to construct binary symbolic dynamics for the system in the usual way: assign the symbol '0' to points to the left of the maximum, '1' to the points to the right. In the period-3 window with the stable cycle $\overline{001}$, the pruning rules are very easy: except for the stable $\overline{001}$ cycle and the $\overline{0}$ fixed point (both disjoint from the invariant set) two zeros in a row are forbidden. In this case it is convenient to redefine the alphabet by denoting the symbol pair 01 by a and the symbol 1 by b. This renders the symbolic dynamics of the points on the repeller complete binary: all sequences of the letters a and b are admissible.

A flow in N dimensions can be reduced to a $(N-1)$-dimensional return map by suspension on a Poincaré section provided that the Poincaré return map is supplemented

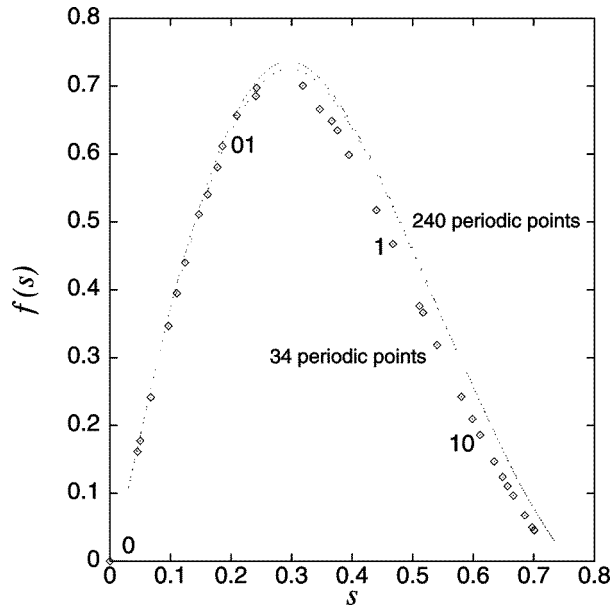

Figure 4. The return map $s_{n+1} = f(s_n)$ constructed from the images of periodic points. The diamonds were obtained by using 34 periodic points, the dots were obtained by using 240 periodic points. We have indicated the periodic points $\overline{0}$, $\overline{1}$ and $\overline{01}$. Note that the transverse fractal structure of the map shows when the number of points is increased. $N = 16$ Fourier modes truncation with $\nu = 0.029\,910$.

by a 'time ceiling function' [21] which accounts for a variation in the section return times. Hence we also determine the return time $T(s_i)$ for each periodic point i, and use those to construct recursively the periodic orbit approximations to the time ceiling function, figure 5. The mean Poincaré section return time is of order $\overline{T} \approx 0.88$.

4.1. Numerical results

We have found all cycles up to topological length 10 (the redefined topological length in the case of the period-3 window), 92 cycles in the chaotic regime and 228 in the period-3 window, by using the one-dimensional parametrization $f(s)$ to find initial guesses for periodic points of the full $N = 16$ Fourier modes truncation and then determining the cycles by a multi-shooting Newton routine. It is worth noting that the effectiveness of using the one-dimensional $f(s)$ approximation to the dynamics to determine initial guesses is such that for a typical cycle it takes only 2–3 Newton iterations to find the cycle with an accuracy of 10^{-10}.

In table 1 we list the periodic orbits to topological length 5 found by our method. The value of Λ_2 serves as an indication of the accuracy of our numerics, as Λ_2 corresponds to the marginal eigenvalue along the periodic orbit, strictly equal to 1. All cycles seem to have real eigenvalues (to within the numerical accuracy) except for the $\overline{0}$-cycle which has a pair of complex eigenvalues, Λ_3 and Λ_4. We therefore do not list the corresponding imaginary parts of the eigenvalues. To illustrate the rapid contraction in the nonleading eigendirections we plot all the eigenvalues of the $\overline{1}$-cycle in figure 6. As the length of the orbit increases, the magnitude of contracting eigenvalues falls quickly below the attainable numerical numerical accuracy $\approx 10^{-16}$ and our numerical results for Λ_k are not meaningful for $k \geqslant 8$.

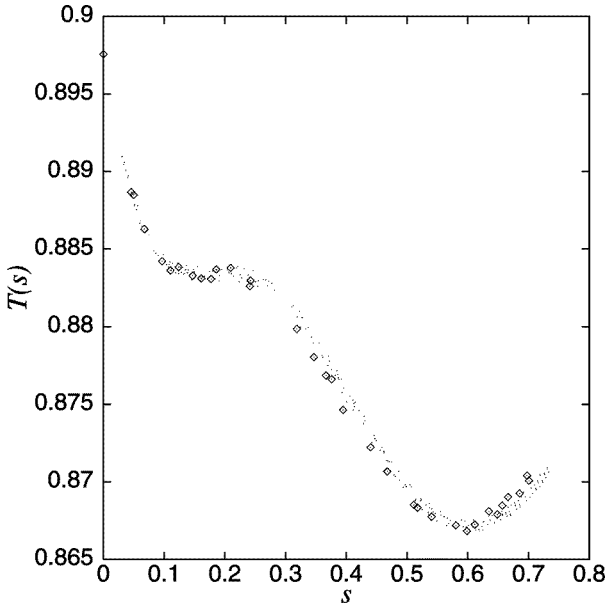

Figure 5. The return time $T(s)$ as a function of the parameter s, evaluated on the periodic points, as in figure 4, with the diamonds obtained by 34 periodic points and the dots by 240 periodic points. The fine structure is due to the fractal structure of the attractor.

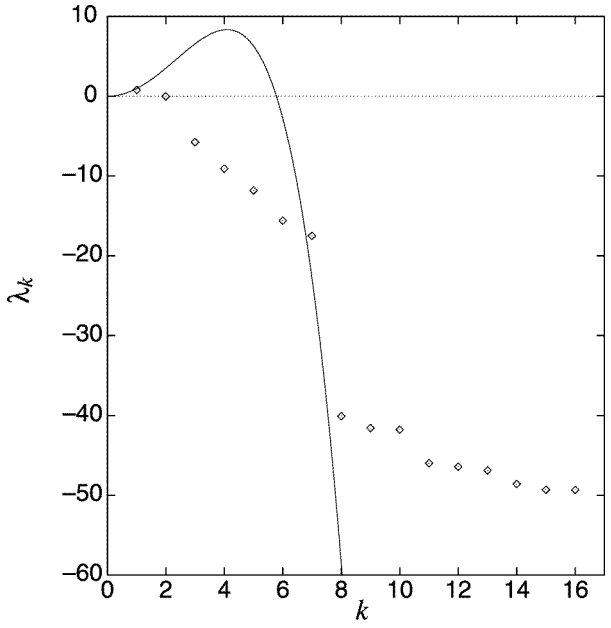

Figure 6. Lyapunov exponents λ_k versus k for the periodic orbit $\bar{1}$ compared with the stability eigenvalues of the $u(x,t) = 0$ stationary solution $k^2 - \nu k^4$. λ_k for $k \geqslant 8$ fall below the numerical accuracy of integration and are not meaningful. $N = 16$ Fourier modes, $\nu = 0.029\,924$, chaotic regime.

Table 1. All cycles up to topological length five for the $N = 16$ Fourier modes truncation of the Kuramoto–Sivashinsky equation (4), damping parameter $\nu = 0.029\,910$ (chaotic attractor) and $\nu = 0.029\,924$ (period-3 window), their itineraries, periods, the first four stability eigenvalues. For the chaotic attractor pruning shows up at the topological length 4; $\overline{0001}$ and $\overline{0011}$ cycles are pruned. The deviation from unity of Λ_2, the eigenvalue along the flow, is an indication of the accuracy of the numerical integration. For the period-3 window we also give the itineraries in the redefined alphabet where $a = 1$ and $b = 10$.

p		T_p	Λ_1	$\Lambda_2 - 1$	Λ_3	Λ_4
Chaotic, $\nu = 0.029\,910$						
0		0.897 653	3.298 183	5×10^{-12}	$-2.793\,085 \times 10^{-3}$	$-2.793\,085 \times 10^{-3}$
1		0.870 729	−2.014 326	-5×10^{-12}	$6.579\,608 \times 10^{-3}$	$-3.653\,655 \times 10^{-4}$
10		1.751 810	−3.801 854	8×10^{-12}	$-3.892\,045 \times 10^{-5}$	$2.576\,621 \times 10^{-7}$
100		2.639 954	−4.852 486	1×10^{-11}	$3.044\,730 \times 10^{-7}$	$-3.297\,996 \times 10^{-10}$
110		2.632 544	6.062 332	2×10^{-11}	$-2.721\,273 \times 10^{-7}$	$-1.961\,928 \times 10^{-10}$
1000		—	—	—	—	—
1100		—	—	—	—	—
1110		3.497 622	−14.767 56	2×10^{-11}	$-1.629\,532 \times 10^{-9}$	$6.041\,192 \times 10^{-14}$
10100		4.393 973	19.643 97	2×10^{-11}	$-1.083\,266 \times 10^{-11}$	$3.796\,396 \times 10^{-15}$
11100		4.391 976	−18.939 79	2×10^{-11}	$1.162\,713 \times 10^{-11}$	$-1.247\,149 \times 10^{-14}$
11010		4.380 100	−26.116 26	2×10^{-11}	$1.005\,397 \times 10^{-11}$	$8.161\,650 \times 10^{-15}$
11110		4.370 895	28.531 33	2×10^{-11}	$1.706\,568 \times 10^{-11}$	$1.706\,568 \times 10^{-14}$
Period-3 window, $\nu = 0.029\,924$						
0		0.897 809	3.185 997	7×10^{-13}	$-2.772\,435 \times 10^{-3}$	$-2.772\,435 \times 10^{-3}$
1	*a*	0.871 737	−1.914 257	5×10^{-13}	$6.913\,449 \times 10^{-3}$	$-3.676\,167 \times 10^{-4}$
10	*b*	1.752 821	−3.250 080	1×10^{-12}	$-4.563\,478 \times 10^{-5}$	$2.468\,647 \times 10^{-7}$
100		2.638 794	−0.315 134	-4×10^{-13}	$4.821\,809 \times 10^{-6}$	$-2.576\,341 \times 10^{-10}$
110	*ab*	2.636 903	2.263 744	3×10^{-12}	$-6.923\,648 \times 10^{-7}$	$-2.251\,226 \times 10^{-10}$
1110	*aab*	3.500 743	−10.871 03	2×10^{-12}	$-2.198\,314 \times 10^{-9}$	$3.302\,367 \times 10^{-14}$
11010	*abb*	4.382 927	−15.841 02	2×10^{-12}	$1.656\,690 \times 10^{-11}$	$1.388\,232 \times 10^{-14}$
11110	*aaab*	4.375 712	18.527 66	3×10^{-12}	$-1.604\,898 \times 10^{-11}$	$2.831\,886 \times 10^{-14}$

Having determined the periodic solutions p in the Fourier modes space, we now go back to the configuration space and plot the corresponding spatiotemporally periodic solutions $u_p(x, t)$: they are the repertoire of the recurrent spatiotemporal patterns that Hopf wanted to see in turbulent dynamics. Different spatiotemporally periodic solutions are qualitatively extremely alike but still different, as a closer inspection reveals. In figure 7 we plot $u_0(x, t)$ corresponding to the Fourier space $\bar{0}$-cycle. Other solutions, plotted in the configuration space, exhibit the same overall gross structure. For this reason we find it more informative to plot the difference $u_0(x, t'T_0) - u_p(x, t''T_p/n_p)$ rather than $u_p(x, t)$ itself. Here p labels a given prime (non-repeating) cycle, n_p is the topological cycle length, T_p its period, and the time is rescaled to make this difference periodic in time: $t' = t/T_0$ and $t'' = n_p t/T_p$, so that t'' ranges from 0 to n_p. $u_0(x, t'T_0) - u_1(x, t''T_1)$ is given in figure 8, and $u_0(x, t'T_0) - u_{01}(x, t''T_{01}/2)$ in figure 9.

5. Global averaging: periodic orbits in action

The above investigation of the Kuramoto–Sivashinsky system demonstrates that it is possible to construct recursively and exhaustively a hierarchy of spatiotemporally periodic unstable solutions of a spatially extended nonlinear system.

Now we turn to the central issue of this paper; qualitatively, these solutions are indeed an

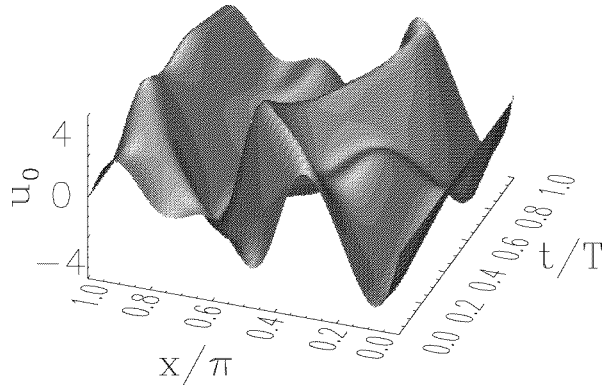

Figure 7. Spatiotemporally periodic solution $u_0(x,t)$. We have divided x by π and plotted only the $x > 0$ part, since we work in the subspace of the odd solutions, $u(x,t) = -u(-x,t)$. $N = 16$ Fourier modes truncation with $\nu = 0.029\,910$.

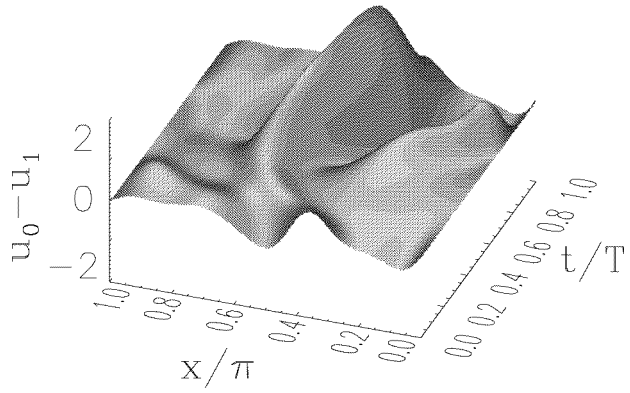

Figure 8. The difference between the two shortest period spatiotemporally periodic solutions $u_0(x, t'T_0)$ and $u_1(x, t''T_1)$.

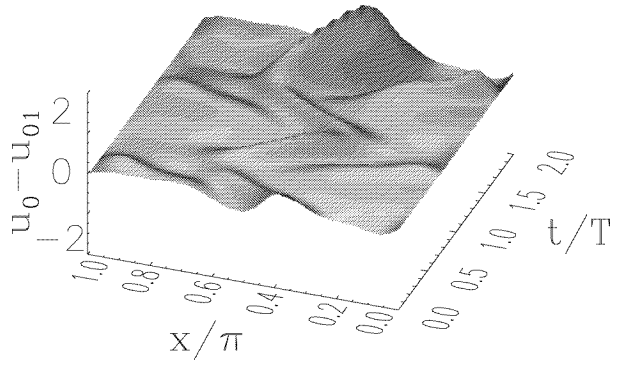

Figure 9. The difference between solution $u_0(x, t'T_0)$ repeated twice and the $n_p = 2$ period spatiotemporally periodic solution $u_{01}(x, t''T_{01}/2)$.

implementation of Hopf's program, but how is this information to be used quantitatively? This is precisely what the periodic orbit theory is about; it offers machinery that puts

together the topological and the quantitative information about individual solutions, such as their periods and stabilities, into predictions about measurable global averages, such as the Lyapunov exponents, correlation functions, and so on. The proper tool for computing such global characterizations of the dynamics are the trace and determinant formulae of the periodic orbit theory.

We shall briefly summarize the aspects of the periodic orbit theory relevant to the present application; for a complete exposition of the theory the reader is referred to [22]. The key idea is to replace a time average $\Phi^t(x)/t$ of an 'observable' ϕ measured along a dynamical trajectory $x(t) = f^t(x)$

$$\Phi^t(x) = \int_0^t \mathrm{d}\tau\, \phi(x(\tau))$$

by the spatial average $\langle \mathrm{e}^{\beta\Phi^t}\rangle$ of the quantity $\mathrm{e}^{\beta\Phi^t(x)}$. Here β is a dummy variable, used to recover the desired expectation value $\langle\phi\rangle = \lim_{t\to\infty}\langle\Phi^t/t\rangle$ by taking $\frac{\mathrm{d}}{\mathrm{d}\beta}$ derivatives of $\langle \mathrm{e}^{\beta\Phi^t}\rangle$ and then setting $\beta = 0$. For large t the average $\langle \mathrm{e}^{\beta\Phi^t}\rangle$ behaves as the trace

$$\operatorname{tr}\mathcal{L}^t = \sum_p T_p \sum_{r=1}^{\infty} \frac{\mathrm{e}^{r\beta\Phi_p}}{|\det(\mathbf{1} - \boldsymbol{J}_p^r)|}\delta(t - rT_p) \tag{5}$$

of the evolution operator

$$\mathcal{L}^t(x, y) = \delta(y - f^t(x))\mathrm{e}^{\beta\Phi^t(x)}$$

and is dominated by its largest eigenvalue $\mathrm{e}^{ts(\beta)}$.

The trace formula (5) has an intuitive geometrical interpretation. The sums in (5) are over prime periodic orbits p and their repeats r, T_p are their periods, and $\boldsymbol{J}_p$ are their stability matrices. Prime cycles partition the dynamical space into closed tubes of length T_p and thickness $|\det(\mathbf{1} - \boldsymbol{J}_p)|^{-1}$, and the trace picks up a periodic orbit contribution only when the time t equals a prime period or its repeat, hence the time delta function $\delta(t - rT_p)$. Finally, $\mathrm{e}^{\beta\Phi_p}$ is the mean value of $\mathrm{e}^{\beta\Phi^t(x)}$ evaluated on this part of dynamical space, so the trace formula is the average of $\langle \mathrm{e}^{\beta\Phi^t}\rangle$ expressed as a partition of the space of solutions into a repertoire of spatiotemporally periodic solutions, each weighted by its stability, i.e. likelihood of its occurrence in a long time evolution of the system.

In applications of the periodic orbit theory the related Fredholm determinant

$$F(\beta, s) = \exp\left(-\sum_p \sum_{r=1}^{\infty} z^{n_p r} \frac{\mathrm{e}^{r(\beta\Phi_p - sT_p)}}{r|\det(\mathbf{1} - \boldsymbol{J}_p^r)|}\right) \tag{6}$$

has better convergence as a function of the maximal cycle length truncation, so that is the function whose leading zero $F(\beta, s(\beta)) = 0$ we determine here in order to evaluate the leading eigenvalue $s(\beta)$.

The dummy variable z in (6) keeps track of the topological lengths n_p (number of the Poincaré section crossings), and is used to expand F as a series in z. If we know all cycles up to topological length l we truncate F to lth order polynomial:

$$F(\beta, s) = 1 - \sum_1^l c_k z^k + (\text{remainder}) \tag{7}$$

and set $z = 1$. The general theory [7, 8, 23] then guarantees that for a hyperbolic dynamical system the coefficients c_k fall off in magnitude exponentially or faster with increasing k. We now calculate the leading eigenvalue $s(\beta)$ by determining the smallest zero of $F(\beta, s)$, and check the convergence of this estimate by studying it as a function of the maximal cycle length truncation l. If the flow conserves all trajectories, the leading eigenvalue must satisfy

$s(0) = 0$; if the invariant set is repelling, the leading eigenvalue yields $\gamma = -s(0)$, the escape rate from the repeller. Once the leading eigenvalue is determined we can calculate the desired average $\langle\phi\rangle$ using formula [6]:

$$\langle\phi\rangle = -\left.\frac{\partial s}{\partial\beta}\right|_{\beta=0} = -\left.\frac{\partial F}{\partial\beta}\right/\left.\frac{\partial F}{\partial s}\right|_{\substack{\beta=0\\ s=s(0)}} . \tag{8}$$

For example, if we take $\log|\Lambda_1^t(x)|$ as our 'observable', the largest eigenvalue of the linearized stability of the flow, Φ_p will be $\log|\Lambda_{1,p}|$ where $\Lambda_{1,p}$ is the largest eigenvalue of stability matrix of the cycle p, and the above formula yields the Lyapunov exponent $\langle\lambda\rangle$.

Both the numerator and the denominator in (8) have a cycle expansion analogous to (7) (cf. [22]), and the same periodic orbit data suffices for their evaluation.

Conceptually the most important lesson of the periodic orbit theory is that the spatiotemporally periodic solutions are *not* to be thought of as eigenmodes to be used as a linear basis for expressing solutions of the equations of motion—as the equations are nonlinear, the periodic solutions are in no sense additive. Nevertheless, the trace formulae and determinants of the periodic orbit theory give a precise prescription for how to systematically explore the repertoire of admissible spatiotemporal patterns, and how to put them together in order to predict measurable observables.

5.1. Numerical results

One of the objectives of a theory of turbulence is to predict measurable global averages over turbulent flows, such as velocity–velocity correlations and transport coefficients. While in principle the periodic orbit averaging formulae should be applicable to such averages, with the present parameter values we are far from any strongly turbulent regime, and here we shall restrict ourselves to the simplest tests of chaotic dynamics: we shall test the theory by evaluating Lyapunov exponents and escape rates.

We compute the periodic orbits, escape rates and Lyapunov exponents both for the period-3 window and a chaotic regime. In the case of period-3 window the complete symbolics dynamics and grammar rules are known and good convergence of cycle expansions is expected both for the escape rate from the repeller and the Lyapunov exponent. Parenthetically, the stable period-3 orbit is separated from the rest of the invariant set by its immediate basin of attraction window, and its eigenvalues bear no immediate relation to the escape rate and the Lyapunov exponent of the repelling set.

In the case of a generic 'strange attractor', the convergence is not expected to be nearly as good, since in this case there exist no finite description of the symbolic dynamics. For closed systems (no escape) $\gamma = 0$ and $F(0, 0) = 0$. The discrepancy of the value $F(0, 0)$ from 0 for a closed system allows us to estimate the accuracy of finite cycle length approximations to the Fredholm determinant.

The analytic properties of the Fredholm determinant are illustrated by the decay rate of the coefficients c_k as a function of k in the expansion (7). If the complete symbolic dynamics is known and the system is hyperbolic, the decay of c_k should be superexponential [7]. This is illustrated in figure 10, where we plot the coefficients c_k for the 16-dimensional system for the chaotic case and for the period-3 window. We can clearly see the superexponential decay for the period-3 window case and at best exponential decay for the chaotic case.

Our results are presented in table 2. One observes that when the symbolic dynamics is known (period-3 window), the convergence is much better than in the generic case, in accordance with the periodic orbit theory expectations.

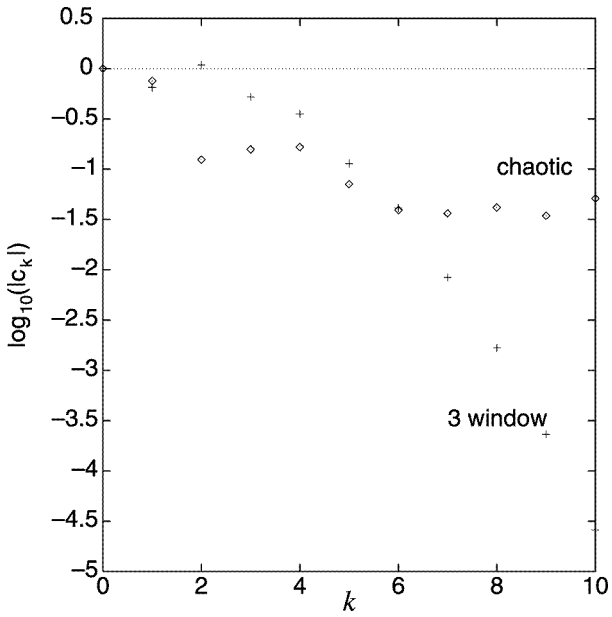

Figure 10. $\log_{10}$ of the coefficients $|c_k|$ in the cycle expansion (7) of $F(0,0)$ versus k for the period-3 window case (crosses) and the chaotic case (diamonds). $N = 16$ Fourier modes truncation.

Table 2. The escape rate γ and the leading Lyapunov exponent as a function of the cycle expansion truncation $n_{\max}$ for the $N = 16$ Fourier modes truncation, chaotic regime ($\nu = 0.029\,910$) and period-3 window ($\nu = 0.029\,924$). In the period-3 window the Fredholm determinant starts converging only for $n_{\max} > 4$; for $n_{\max} = 4$ it has no real zero at all. A numerical simulation estimate for the Lyapunov exponent in the chaotic regime is given in the last line; for this parameter value the escape rate, γ, should strictly equal zero.

	Chaotic		Period-3 window	
$n_{\max}$	γ	λ_1	γ	λ_1
1			0.428 143	0.703 010
2	0.441 948	0.981 267	−0.187 882	0.430 485
3	0.080 117	0.765 050	−0.049 325	0.469 350
4	0.148 583	0.703 072		
5	0.068 513	0.727 498	1.072 468	0.585 506
6	0.027 724	0.699 907	0.078 008	0.547 005
7	0.035 137	0.693 852	0.088 132	0.598 977
8	0.007 104	0.675 529	0.090 425	0.631 551
9	0.021 066	0.673 144	0.090 101	0.618 160
10	0.007 367	0.646 233	0.090 065	0.621 271
Numer.		0.629		

6. Summary

Hopf's proposal for a theory of turbulence was, as we understand it, to think of turbulence as a sequence of near recurrences of a repertoire of unstable spatiotemporal patterns. Hopf's proposal is in its spirit very different from most ideas that animate current turbulence

research. It is distinct from the Landau quasiperiodic picture of turbulence as a sum of infinite number of incommensurate frequencies, with dynamics taking place on a large-dimensional torus. It is not the Kolmogorov's 1941 homogeneous turbulence with no coherent structures fixing the length scale, here all the action is in specific coherent structures. It is emphatically *not* universal; spatiotemporally periodic solutions are specific to the particular set of equations and boundary conditions. And it is *not* probabilistic; everything is fixed by the deterministic dynamics with no probabilistic assumptions on the velocity distributions or external stochastic forcing.

Our investigation of the Kuramoto–Sivashinsky system is a step in the direction of implementing Hopf's program. We have constructed a complete and exhaustive hierarchy of spatiotemporally periodic solutions of spatially extended nonlinear system and applied the periodic orbit theory to evaluation of global averages for such system. Conceptually the most important lesson of this theory is that the unstable spatiotemporally periodic solutions serve to explore systematically the repertoire of admissible spatiotemporal patterns, with the trace and determinant formulae and their cycle expansions being the proper tools for extraction of quantitative predictions from the periodic orbits data.

We have applied the theory to a low-dimensional attractor, not larger than the Lorenz's original strange attractor [24]. As our aim was to solve the given equations accurately, we were forced to work with a high-dimensional Fourier modes truncations, and we succeeded in determining the periodic orbits for flows of much higher dimension than in previous applications of the periodic orbit theory. As something new, we have developed an intrinsic parametrization of the invariant set that provided the key to finding the periodic orbits.

In practice, the method of averaging by means of periodic orbits produced best results when the complete symbolic dynamics was known. For generic parameter values we cannot claim that the periodic orbit approach is computationally superior to a direct numerical simulation. A program to find periodic orbits up to length 10 for one value of the damping parameter ν requires a day of CPU on a fast workstation, much longer than the time used in the direct numerical simulations.

The parameter ν values that we work with correspond to the weakest nontrivial 'turbulence', and it is an open question to what extent the approach remains implementable as the system goes more turbulent. Our hope is that the unstable structures captured so far can be adiabatically tracked to the 'intermediate turbulence' regime, and still remain sufficiently representative of the space of admissible patterns to allow meaningful estimates of global averages. As long as no effective method for constructing intrinsic coordinates for the 'inertial manifold' exists and we rely on the spatial Fourier decomposition, the present approach is bound to fail in the 'strong turbulence' $\nu \to 0$ limit, where the dominant structures are Burgers-type shocks and truncations of the spatial Fourier modes expansions are increasingly uncontrollable.

Acknowledgments

We are grateful to L Tuckerman for patient instruction, E A Spiegel, G Goren, R Zeitek, I Procaccia for inspiring conversations, P Dahlqvist for a critical reading of an early version of the paper, and E Bogomolny for the catchy but all too ephemeral title for the paper.

References

[1] Cvitanović P (ed) 1992 Periodic orbit theory—theme issue *CHAOS* **2** 1–158
[2] Moss F 1994 Chaos under control *Nature* **370** 615

[3] Kuramoto Y and Tsuzuki T 1976 Persistent propagation of concentration waves in dissipative media far from thermal equilibrium *Prog. Theor. Phys.* **55** 365
[4] Sivashinsky G I 1977 Nonlinear analysis of hydrodynamical instability in laminar flames—I. Derivation of basic equations *Acta Astron.* **4** 1177
[5] Cvitanović P 1988 *Phys. Rev. Lett.* **61** 2729
[6] Artuso R, Aurell E and Cvitanović P 1990 Recycling of strange sets I: Cycle expansions *Nonlinearity* **3** 325
[7] Rugh H H 1992 The correlation spectrum for hyperbolic analytic map *Nonlinearity* **5** 1237
[8] Cvitanović P, Rosenqvist P E, Rugh H H and Vattay G 1993 A Fredholm determinant for semiclassical quantization *CHAOS* **3** 619
[9] Poincaré H 1892–99 *Les méthodes nouvelles de la méchanique céleste* (Paris: Guthier-Villars)
[10] Hopf E 1942 Abzweigung einer periodischen Lösung *Bereich. Sächs. Acad. Wiss. Leipzig, Math. Phys. Kl.* **94** 19
[11] Moore D W and Spiegel E A 1966 A thermally excited nonlinear oscillator *Astrophys. J.* **143** 871
[12] Baker N H, Moore D W and Spiegel E A 1971 *Quatr. J. Mech. Appl. Math.* **24** 391
[13] Spiegel E A 1987 Chaos: a mixed metaphor for turbulence *Proc. R. Soc.* A **413** 87
[14] Kevrekidis I G, Nicolaenko B and Scovel J C 1990 Back in the saddle again: a computer assisted study of the Kuramoto–Sivashinsky equation *SIAM J. Appl. Math.* **50** 760
[15] See e.g. Foias C, Nicolaenko B, Sell G R and Témam R 1988 Kuramoto–Sivashinsky equation *J. Math. Pures Appl.* **67** 197
[16] Goren G, Eckmann J-P and Procaccia I A Scenario for the Onset of Spacetime Chaos unpublished
[17] Cvitanović P and Eckhardt B 1993 Symmetry decomposition of chaotic dynamics *Nonlinearity* **6** 277
[18] We thank Laurette Tuckerman for providing us with the pseudospectral code
[19] We have used the NAG library integration routine D02BHF. Our code and numerical results are available on `http://www.nbi.dk/~predrag/QCcourse/`
[20] Dellnitz M, Golubitsky M and Nicol M 1994 Symmetry of attractors and the Karhunen–Loéve decomposition *Appl. Math. Sci.* **100** 73
Golubitsky M and Nicol M 1995 Symmetry detectives for SBR attractors *Nonlinearity* **8** 1027
[21] Bowen R 1975 *Equilibrium States and the Ergodic Theory of Anosov-diffeomorphisms (Springer Lecture Notes in Mathematics 470)* (Berlin: Springer)
[22] Cvitanović P *et al* 1996 *Classical and Quantum Chaos—Periodic Orbit Theory* textbook in preparation `http://www.nbi.dk/~predrag/QCcourse/`
[23] Ruelle D 1978 *Statistical Mechanics, Thermodynamic Formalism* (Reading, MA: Addison-Wesley)
[24] Lorenz E N 1963 Deterministic nonperiodic flow *J. Atmos. Sci.* **20** 130